Influence of Cusp External Magnetic Field on Deposition Rate of Two-electrode TIG Welding

Liming Liu (liulm@dlut.edu.cn)
Key Laboratory of Liaoning Advanced Welding and Joining Technology
Yanli Zhu
Key Laboratory of Liaoning Advanced Welding and Joining Technology
Runtao Liu
Key Laboratory of Liaoning Advanced Welding and Joining Technology

Research Article

Keywords: T-TIG, Cusp EMF, Deposition rate, Arc shape, Arc energy

Posted Date: October 26th, 2021

DOI: https://doi.org/10.21203/rs.3.rs-1007000/v1

Version of Record: A version of this preprint was published at The International Journal of Advanced Manufacturing Technology on January 21st, 2022. See the published version at https://doi.org/10.1007/s00170-022-08706-2.

Influence of cusp external magnetic field on deposition rate of two-electrode TIG welding

Liming Liu [1] • Yanli Zhu [1] • Runtao Liu [1]

[1] Liaoning Key Laboratory of Advanced Welding and Joining Technology, School of Materials Science and Engineering, Dalian University of Technology, Dalian 116024, China

Corresponding author: Liming Liu

Email: liulm@dlut.edu.cn

Abstract

Experiments have been conducted to investigate the influence of the cusp external magnetic field (EMF) on deposition rate of two-electrode tungsten insert gas (T-TIG) welding. T-TIG arc parameters such as arc shape, arc voltage, arc pressure and arc plasma information were acquired respectively. Results showed compared to TIG, a higher welding current could be allowed for T-TIG, due to its low arc pressure characteristic. Under the effect of the cusp EMF, the arc shape was compressed along *x*-axis of T-TIG, while elongated along *y*-axis of T-TIG. Besides, the peak arc pressure of T-TIG was not significantly increased by the cusp EMF. Moreover, with the action of the cusp EMF, the maximum values of the electron temperature (T_e) and electron density (N_e) of T-TIG were not significantly increased, but along *y*-axis, the increments of the two parameters were gradually increased and their distributions were widened. Therefore, more arc energy was allocated on *y*-axis of T-TIG by the cusp EMF, which could improve the preheating and the melting of the filler wire along *y*-axis, so the deposition rate of T-TIG could be increased by 17.6% under the effect of the cusp EMF.

Keywords T-TIG • Cusp EMF • Deposition rate • Arc shape • Arc energy

1 Introduction

Tungsten insert gas (TIG) welding has advantages of low cost, simple operation and high weld quality, and has been widely used in manufacturing industry. However, low deposition

rate of TIG could not meet the demand for higher productivity in modern manufacturing industry [1, 2]. Previously, a two-electrode TIG (T-TIG) welding method was proposed to improve the welding efficiency [3]. In this welding method, a bigger hybrid arc was generated by the two electrodes with small distance and insulated from each other, which was a novel welding heat source different from TIG.

Many researchers have utilized T-TIG welding method to achieve high deposition rate and high welding efficiency welding process. Kobayashi et al. [4] employed T-TIG to weld the special equipment with large volume and thick wall, and achieved welding process with consistent penetration and high deposition rate. Leng et al. [5,6] proposed that the arc pressure of T-TIG was considerably lower than that of single TIG under the similar heat input, so T-TIG could be employed to weld thick plate with high deposition rate due to its stable weld pool under high current. Qin and Jiang et al. [7,8] proposed tandem pulsed gas tungsten arc welding (GTAW-P), in which the main arc at pulse peak achieved sufficient penetration and the assisting arc at pulse background reduced the unnecessary heat input, and found that compared with the single and tandem GTAW, the heat input of tandem GTAW-P was decreased by 17.5% and 14.5% respectively. Wu et al. [9] developed the coupled numerical models of electrode, arc and weld pool for TIG and tandem TIG welding, and found that the arc interaction in tandem TIG caused the arc expansion and decrease of current density, and thus the maximum arc temperature and arc plasma flow velocity of the tandem TIG were only slightly larger than those of the single TIG, even though the leading arc current was much larger. In summary, T-TIG can achieve high deposition rate welding in some production field, but the expanded arc shape of T-TIG leads to a low energy utilization rate, which is not conducive to further increase its deposition rate. Therefore, it is the key to further improve the deposition rate of T-TIG that how to make good use its energy.

Since the arc plasma is a good electromagnetic conductor, it is an effective way to modify

its thermal-force behaviour by external magnetic field (EMF). The cusp EMF is generated by four magnetic poles in form of excitation coils or permanent magnets, which can constrain the arc plasma [10]. Liu et al. [11, 12] observed that after the cusp EMF was applied, the area of the melted zone of K-TIG was reduced and its shape became ellipse, and they also indicated that the pole angle of magnetic field generator had important influence on melted zone area and weld penetration. The authors' research group have made the initial experiment to investigate the effect of a cusp EMF on T-TIG welding process, and pointed out that the cusp EMF could make the electron density of low-current T-TIG increased by 16%, so the physical property of the common conductive zone of the T-TIG was improved [13]. However, the effect of the cusp EMF on the deposition rate of T-TIG, especially high-current T-TIG, has not yet been investigated.

In this study, the influence of the cusp EMF on the thermal-force behaviour of T-TIG was experimentally studied, to investigate the energy allocation of T-TIG by the cusp EMF and further reveal the mechanism of the cusp EMF enhanced the deposition rate of T-TIG.

2 Experimental methods

Fig. 1 shows the welding system schematic diagram of T-TIG assisted by a cusp EMF. Two welding power sources were used to power the two electrodes respectively, which could be adjusted independently. When welding, the electrodes remained stationary, while the workpiece moved. There were two kinds of workpieces, one was a water-cooled copper plate used for arc shape and arc spectrum acquisition process, the other was a Q235B steel plate used for bead-on-plate welding. The filler wire (ER50-6) with a diameter of 1.2 mm was fed along *y*-axis, which was perpendicular to the array of the two electrodes shown in Fig. 1. Table 1 shows the detailed process parameters. A voltage sensor was connected to the electrode and the workpiece, and then the acquired voltage signal was transferred to the A/D converter by a data acquisition (DAQ) card, and consequently the digital voltage signal was obtained. A

pressure sensor with a measuring range of 0-5 kPa was installed under a water-cooled copper block with a 1 mm diameter hole shown in Fig. 1. The arc acted on the pressure sensor after passing through the hole, and then the pressure signal was acquired by the DAQ card. A high-speed camera was employed to acquire the arc shape. In this experiment, the settings of the high-speed camera were 320×240 pixel resolution, 500 μs exposure time and 2000 frame/s acquiring frequency. A spectrograph (SP-2556) was employed to acquire arc plasma information. The 300 grove/mm grating with 0.128 nm resolution was selected to acquire the arc spectrum within the range from 400 nm to 900 nm. The acquired spectrum of arc plasma is shown in Fig. 2.

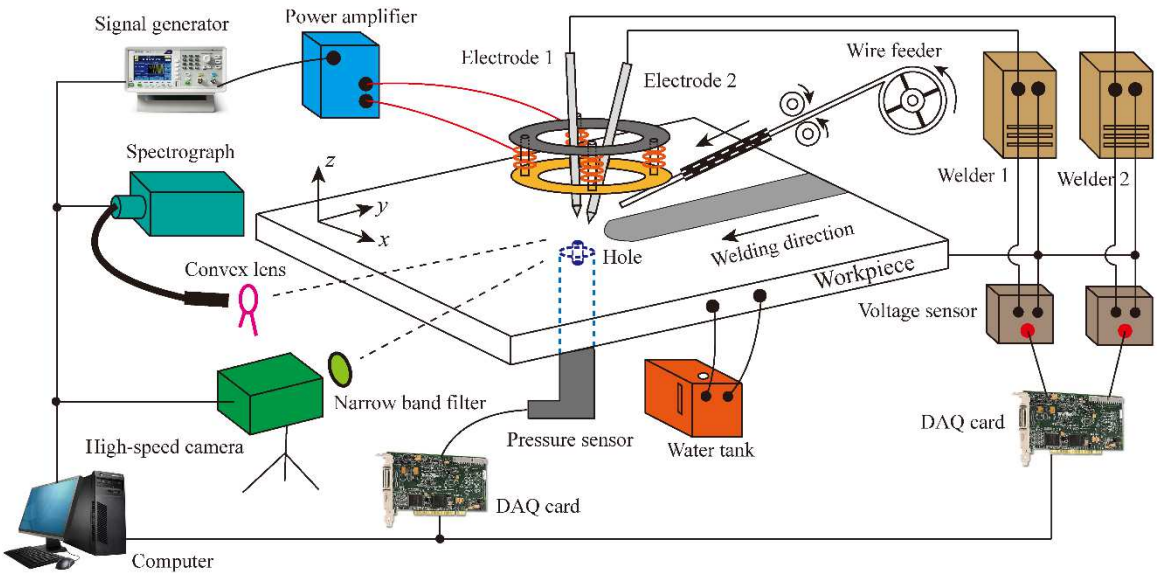

Fig. 1 T-TIG welding process assisted by a cusp external magnetic field

Table 1 Welding parameters

Parameter	TIG	T-TIG
Welding current (A)	150, 300	150+150
Electrode diameter (mm)	3.2	3.2
Electrode distance (mm)	–	2
Electrode height (mm)	5	5
Electrode connection	DCEN	DCEN
Welding velocity (mm/s)	4	4
Shielding gas, Ar (L/min)	15	15
Excitation current (A)	50	50
Magnetic flux density (mT)	58	58

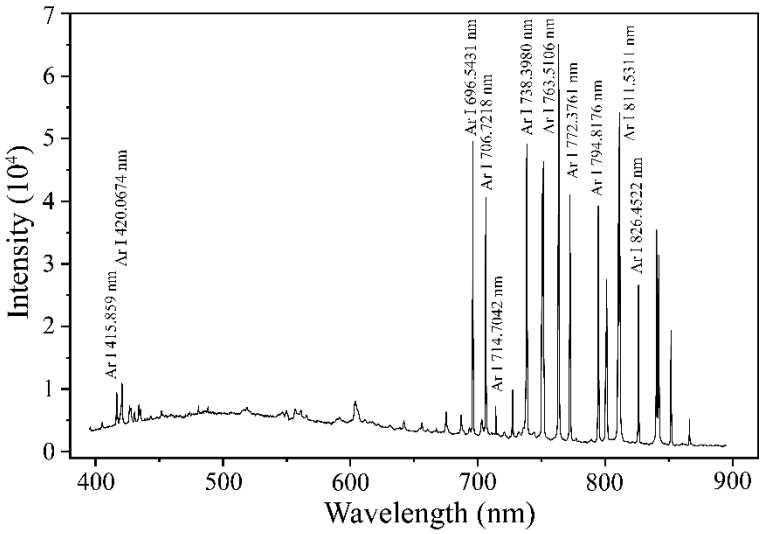

Fig. 2 Arc plasma spectrum from 400 nm to 900 nm.

A self-designed cusp EMF generator consisted of four core columns distributed in a circular array, and each was twined with 12 turns of copper coils as shown in Fig. 3. A signal generator was employed to direct the power amplifier that was used to power the coils as illustrated in Fig. 1. The twined direction of the coils located at two opposite core columns was same, while it was converse when the coils were located at two adjacent core columns., which could produce a cusp EMF like N-S-N-S. The more detailed information about the magnetic-field generator was discussed in the reference [13].

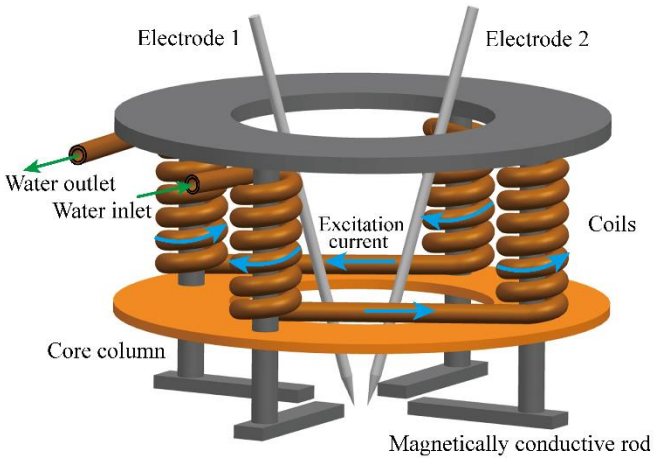

Fig. 3 The cusp external magnetic field generator

3. Experimental results

3.1 Low arc pressure characteristic of T-TIG

Arc shapes of TIG and T-TIG are shown in Fig. 4. As shown in Fig. 4(a, b), the TIG arc shape was typical bell-shaped and expanded when the current increased from 150 A to 300 A. For T-TIG, the arc shape was different along *x*-axis and *y*-axis as shown in Fig. 4(c, d). Along *x*-axis, T-TIG (150A+150A) nearly had the same outline as TIG (300A) near the workpiece, while the outline of the former was wider than the latter near the electrodes. This was mainly because the electrons were emitted from two electrodes and thus a larger cathode region was formed for the T-TIG. Besides, the arc voltage of the T-TIG was slightly higher than that of TIG (150A), but nearly 20.3% lower than that of TIG (300A).

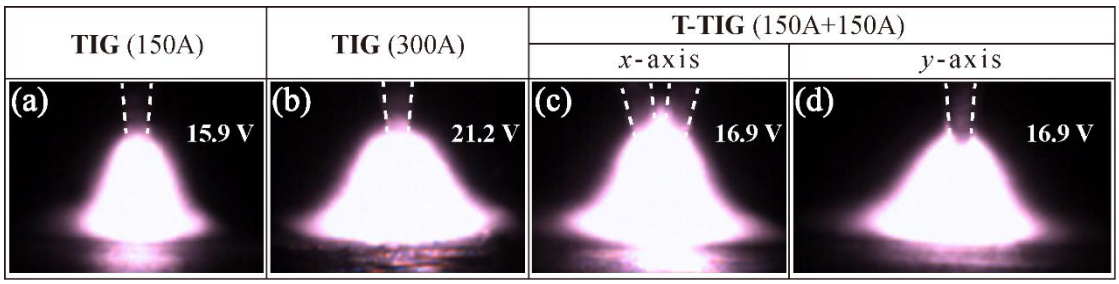

Fig. 4 Arc shapes: **a** TIG with 150 A; **b** TIG with 300 A; **c,d** T-TIG with 150A+150A

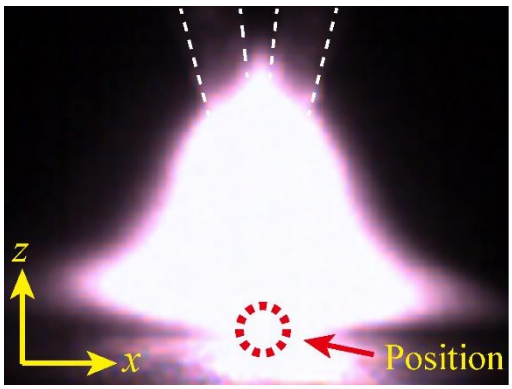

Fig. 5 Arc pressure acquisition position

Arc pressure was a significant physical parameter of welding arc, and especially the peak arc pressure had a crucial effect on weld pool status and weld bead formation [6,14]. For T-TIG, when the electrode distance was small, the arc pressure distribution was in concordance with Gaussian distribution [15]. Therefore, in this experiment, the acquisition position of the peak arc pressure is shown in Fig. 5. The measured peak arc pressures of TIG and T-TIG are shown in Fig. 6. The peak arc pressure of T-TIG (150A+150A) was 221 Pa, which was only

slightly higher than that of TIG (150A), even though the current of the former were two times greater than the latter, but nearly 83% lower than that of TIG (300A), even though the currents of the both were equal.

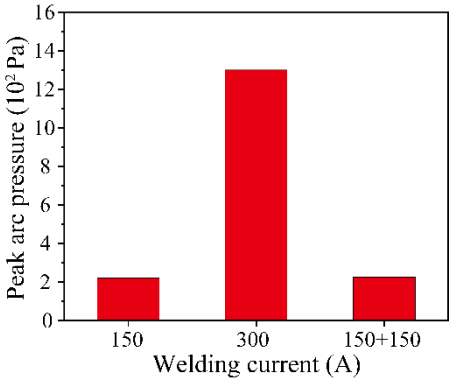

Fig. 6 Peak arc pressures of TIG (150A), TIG (300A) and T-TIG (150A+150A)

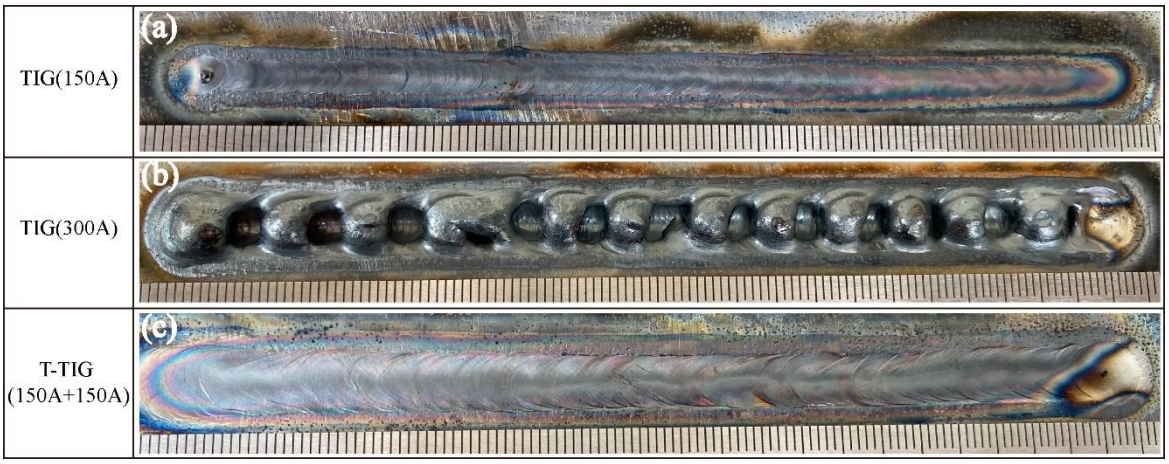

Fig.7 Weld appearances without filler wire: **a** TIG with 150A; **b** TIG with 300A; **c** T-TIG with 150A+150A

The weld bead formations without filler wire of TIG and T-TIG are shown in Fig. 7. As shown in Fig. 7(a, c), the sound weld bead formations were obtained for TIG (150 A) and T-TIG (150A + 150A) respectively, and the weld bead width of the latter was larger than the former, because of its higher heat input. However, the weld defect of humping occurred for TIG (300 A). The humping defect of weld pool was closely associated with the extremely high arc pressure based on experimental observation and analytical calculation [14,16]. Therefore, it was limited that improving the deposition rate of TIG by simply increasing welding current, while a higher welding current could be allowed for T-TIG, due to its low arc pressure characteristic, which caused T-TIG had the potential to obtain higher deposition rate.

3.2 Effect of EMF on deposition rate

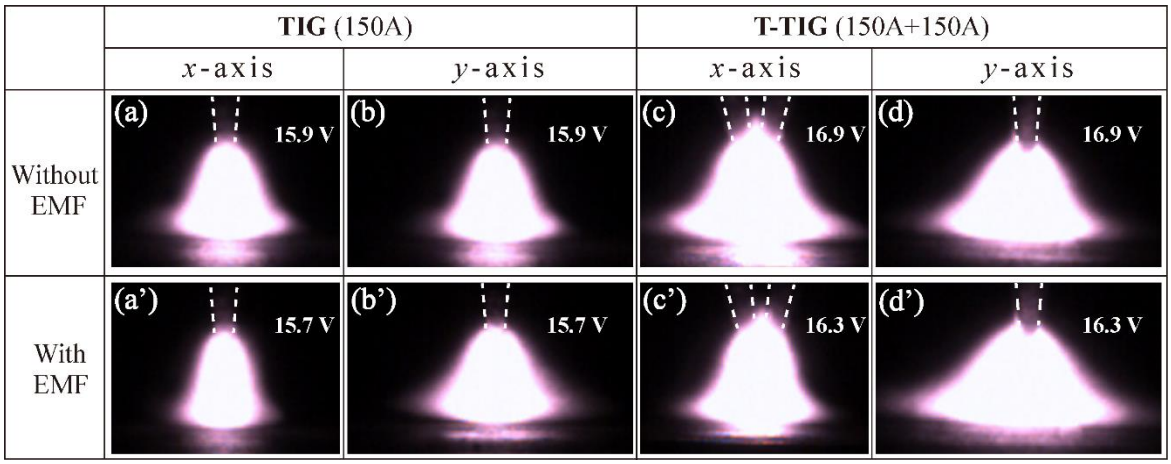

Fig. 8 Arc shapes: **a,b** TIG (150A); **a',b'** TIG (150A) with EMF; **c,d** T-TIG (150A+150A); **c',d'** T-TIG (150A+150A) with EMF

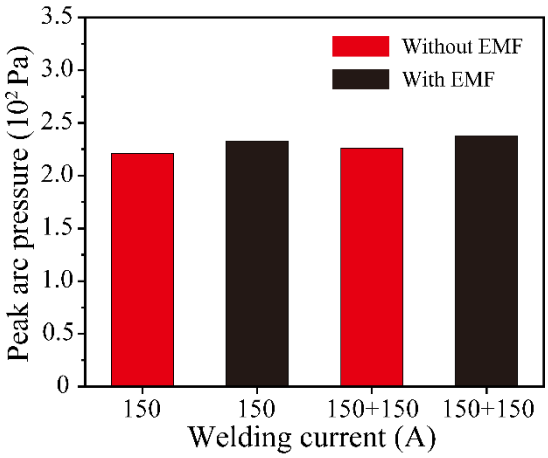

Fig. 9 Peak arc pressures of TIG (150A) and T-TIG (150A+150A) with and without EMF

The arc shapes of TIG and T-TIG with the cusp EMF are shown in Fig. 8. Under the effect of the cusp EMF, the arc shapes of TIG and T-TIG were obviously compressed along *x*-axis as shown in Fig. 8(a', c'), while elongated along *y*-axis as shown in Fig. 8(b', d'). Besides, the arc voltages of TIG and T-TIG were not significantly changed. The measured peak arc pressures of TIG and T-TIG with the cusp EMF are shown in Fig. 9. It could be seen that the peak arc pressures of TIG and T-TIG were only slightly increased under the effect of the cusp EMF.

Electron temperature (T_e) and electron density (N_e) were the internal properties of welding arc, which represented the discharge state of the arc plasma and also influenced the welding

process. By acquiring and analyzing the arc plasma spectrum information, the change law of the magnitudes and distributions of T_e and N_e could be acquired, which was beneficial to reveal the influence mechanism of the cusp EMF on arc plasma. For TIG and T-TIG, the arc shapes were axisymmetric along both x-axis and y-axis as shown in Fig. 8, and thus, for convenience, only a half of the arc was selected to acquire arc spectrum. Moreover, to further reduce the influence of workpiece evaporation on the arc plasma, the arc spectrum located 2 mm above the workpiece was acquired by a 1 mm step, as illustrated in Fig. 10.

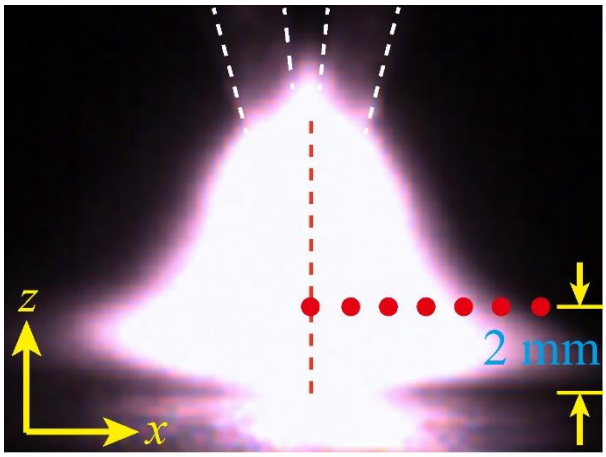

Fig. 10 Spectrum acquisition positions on arc plasma

T_e and N_e of arc plasma could be estimated according to mathematic and physical theories, mainly including Boltzmann plot method and Stark broadening effect in spectrum diagnose, on the assumption that the arc plasma was local thermal equilibrium and optically thin [17-21]. In order to ensure the calculation precision, the upper level energy of the selected spectrum lines should meet the following criterion [22,23],

$$E_{m1} - E_{m2} > kT_e \tag{1}$$

where E_m is the upper level energy, k is the Boltzmann constant. In this experiment, spectrum lines of Ar I 415.859 nm, Ar I 420.0674 nm, Ar I 696.5431 nm, Ar I 706.7218 nm, Ar I 714.7042 nm and Ar I 772.3761 nm were selected for calculating electron temperature, and the physical parameters of these spectrum lines are shown in Table 2 [24]. Stark broadening of a certain spectrum line spontaneously emitted by particles in the plasma was convenient for

determining the electron density after the electron temperature was obtained. In order to acquire the spectrum line profile with the best quality, a 2400 grove/mm grating with the resolution of 0.011 nm was selected. Spectrum line of Ar I 696.5431 nm was selected to calculate electron density.

Table 2 Physical parameters of spectrum lines [24]

Wavelength, λ (nm)	Transition	Transition probability, A ($10^8 s^{-1}$)	Upper level energy, E (eV)	Statistical weight of upper level, g
415.859	$5p^2[3/2]_2$—$4s^2[3/2]^0_2$	0.014	14.5289	5
420.0674	$5p^2[5/2]_3$—$4s^2[3/2]^0_2$	0.0097	14.4990	7
696.5431	$4p^2[1/2]_1$—$4s^2[3/2]^0_2$	0.064	13.3278	3
706.7218	$4p^2[3/2]_2$—$4s^2[3/2]^0_2$	0.038	13.3022	5
714.7042	$4p^2[3/2]_1$—$4s^2[3/2]^0_2$	0.0063	13.2826	3
772.3761	$4p^2[3/2]_1$—$4s^2[3/2]^0_2$	0.052	13.1531	3

The distribution of T_e and N_e of TIG (150A) and T-TIG (150A+150A) along x-axis and y-axis are shown in Fig. 11. For TIG and T-TIG, the maximum values of T_e and N_e were both located at the central axis of the arc, and they gradually decreased as the radial distance increased. It should be pointed out that the maximum values of T_e and N_e of the T-TIG were only slightly higher than the TIG, although the current of the former was two times greater than the latter. This might be the main reason that the peak arc pressure of the T-TIG was not obviously greater than the TIG.

As shown in Fig. 11, after the cusp EMF was applied, the maximum values of T_e and N_e of T-TIG were not significantly increased, but they showed different changes along x-axis and y-axis. Along x-axis, the distributions of T_e and N_e of T-TIG became more concentrated and their change gradients were increased. While along y-axis, the distribution of T_e and N_e of T-TIG became wider, and the values of the two parameters were increased at each position. Moreover, it was noteworthy that the increments of the two parameters mentioned above were both gradually increased as the radial distance increased. Additionally, T_e and N_e of TIG

showed similar change law to T-TIG under the effect of the cusp EMF. Therefore, the cusp EMF could change the arc energy allocation of TIG and T-TIG, so more arc energy was allocated on *y*-axis.

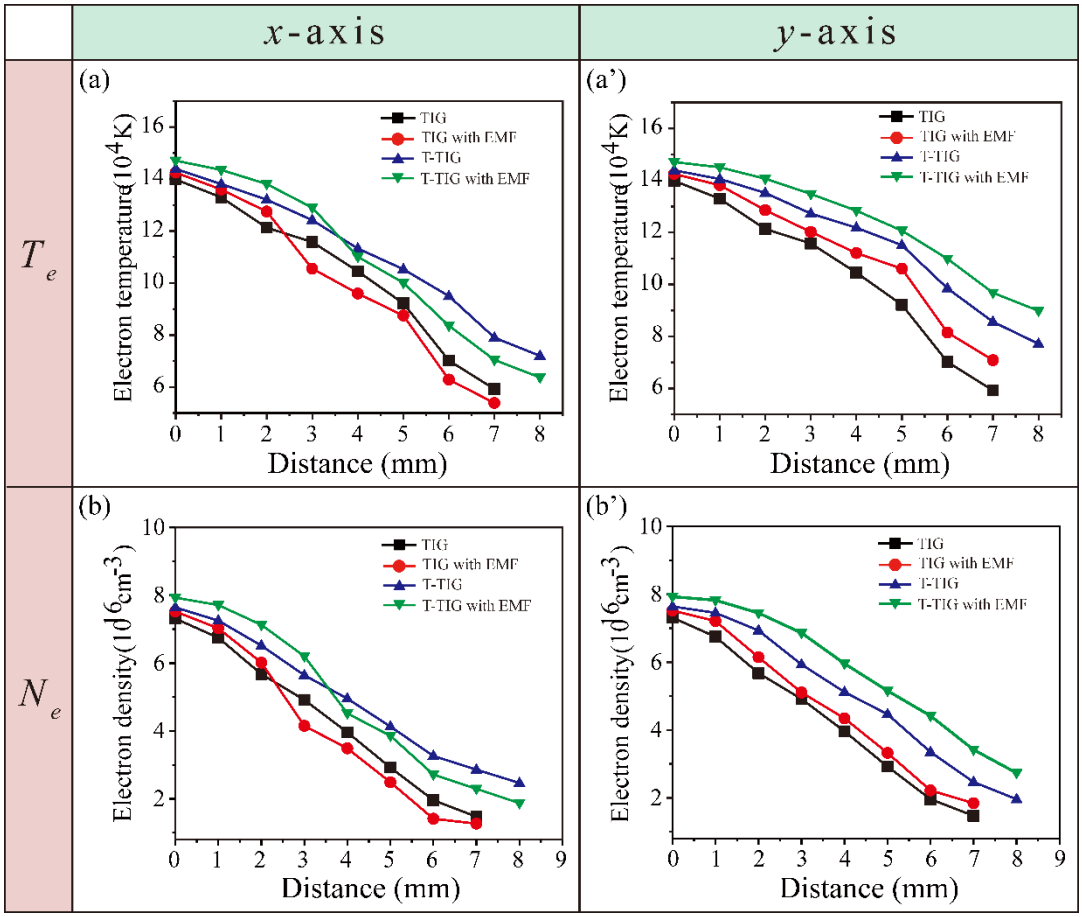

Fig. 11 a,a' Electron temperature and **b,b'** electron density distribution of TIG (150A) and T-TIG (150A+150A) with and without EMF.

In order to better observe the influence of the cusp EMF on the deposition rate, the filler wire was fed along y-axis. The weld bead appearances of TIG (150A) and T-TIG (150A+150A) with different wire feeding speeds (WFS) and the allowed maximum WFS in this experiment are shown in Fig. 12 and Fig. 13 respectively. For the TIG, when the WFS did not exceed 90 cm/min, a continuous and sound weld bead was achieved. Otherwise, the width of the weld beads became uneven. However, as the cusp EMF was applied, the humping weld defect just occurred when the WFS exceeded 100 cm/min. Therefore, the deposition rate of the TIG could be increased by 11% under the effect of the cusp EMF. Compared to the TIG, the spreadability

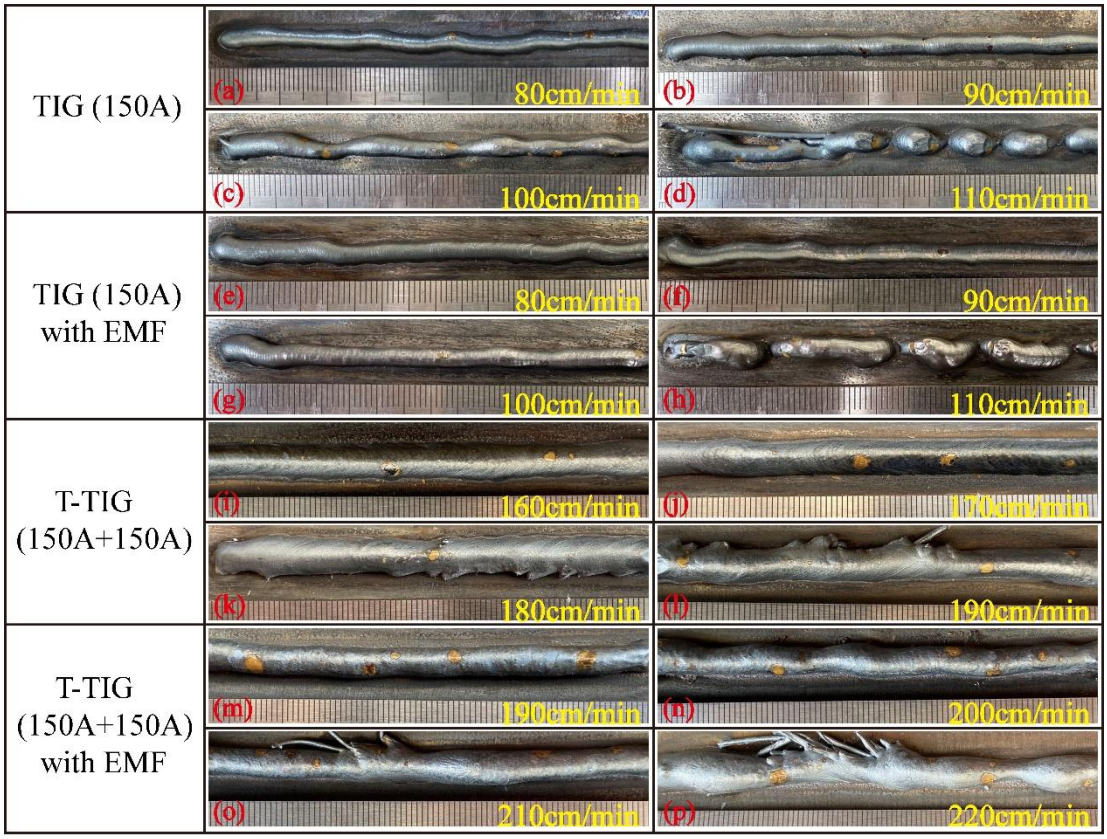

Fig. 12 Weld formations under different wire feeding speeds: **a,b,c,d** TIG (150A); **e,f,g,h** TIG (150A) with EMF; **i,j,k,l** T-TIG (150A+150A); **m,n,o,p** T-TIG (150A+150A) with EMF

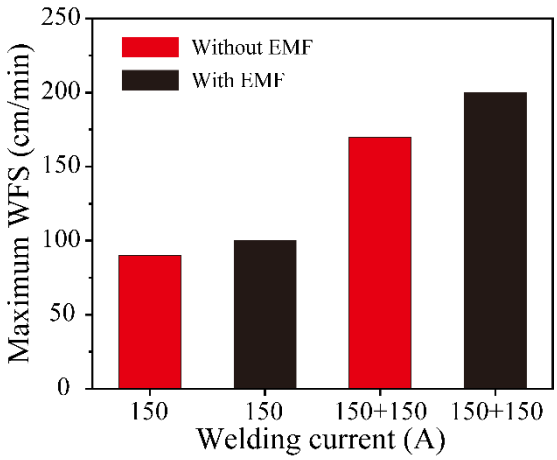

Fig. 13 Maximum wire feeding speeds of TIG (150A) and T-TIG (150A+150A) with and without EMF

of weld bead of the T-TIG was better due to its higher heat input. When the WFS did not exceed 170 cm/min, a continuous and smooth weld bead was achieved, while when the WFS reached 180 cm/min, the weld bead became uneven, and even the filler wire was not completely melted. However, after the cusp EMF was applied, the weld bead still remained continuous, even when the WFS reached 200 cm/min. Therefore, the deposition rate of the T-TIG could be increased

by 17.6% under the effect of the cusp EMF. This was mainly because the arc energy allocation of T-TIG was optimized, and thus the preheating and the melting of the filler wire was improved.

4. Discussions

4.1 Allocation mechanism of arc energy by EMF

Based on the above experimental results, it could be concluded that the cusp EMF contributed to the improvement of the deposition rate of T-TIG mainly by changing arc energy allocation. Therefore, it was necessary to further analyze the influence of the cusp EMF on the arc plasma behaviour, aimed to reveal the allocation mechanism of the arc energy by the cusp EMF. Fig. 14 shows the schematics of magnetic field distribution around T-TIG and the force analysis. As illustrated in Fig. 15, to better demonstrate the influence of the cusp EMF on arc plasma, a charged particle was selected for force analysis. For each electrode arc of T-TIG, the self-magnetic contraction force F_E and the electromagnetic force F_D from the other electrode arc could be expressed as follows [25,26],

$$F_E = J(r) \times B(r) \tag{2}$$

$$F_D = J(r) \times B_D \tag{3}$$

where r is the position of the charged particle, $J(r)$ is the arc current density, $B(r)$ is the self-induced magnetic flux density, B_D is the magnetic flux density induced by the other electrode arc. The direction of F_E pointed to the central axis of each electrode arc, and the direction of F_D pointed to the central axis of the two electrodes.

Under the actions of F_E and F_D, the charged particles of T-TIG moved to the central axis of the two electrodes at high speed along x-axis, so the two arcs attracted each other and formed a coupled arc. Meanwhile, violent collisions occurred among the charged particles on the central axis, which caused a large number of the charged particles moved outward along y-axis, except that some of the charged particles moved along the central axis. This was because the

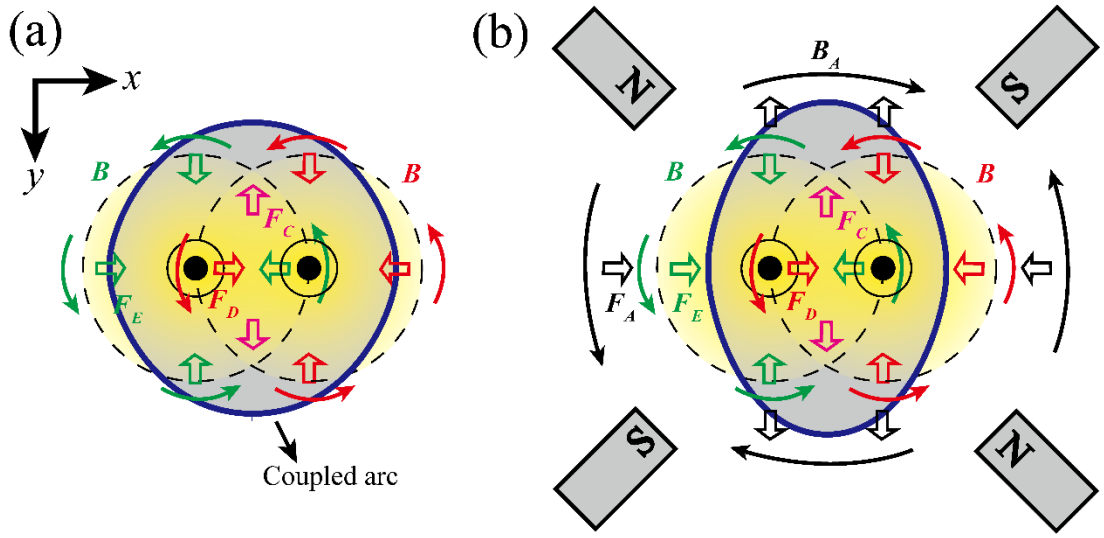

Fig. 14 Schematic of magnetic field distribution and force analysis on *xOy* cross section: **a** T-TIG; **b** T-TIG with EMF

movement space of the charged particles was relatively free along *y*-axis, compared to their movement space along the central axis. Therefore, along *y*-axis, the collision force F_C acting on the charged particles was not negligible except F_E and F_D, and the direction of F_C pointed to the periphery of the coupled arc as illustrated in Fig. 14(a).

It could be seen from Fig. 14(b) that the cusp EMF around T-TIG consisted of two clockwise N→S magnetic paths and two counterclockwise N→S magnetic paths. When the cusp EMF was applied, the additional electromagnetic force F_A could be expressed as follow,

$$F_A = J(r) \times B_A \tag{4}$$

where B_A is the external magnetic flux density. The direction of F_A pointed to the central axis of the coupled arc along *x*-axis, while pointed to the periphery of the coupled arc along *y*-axis as illustrated in Fig. 14(b).

Along *x*-axis, under the effect of F_A, the charged particles accelerated toward the central axis of the coupled arc, and then the coupled arc was compressed. Meanwhile, the collision among the charged particles on the central axis was also strengthened, which further improved collision ionization and increased the electron density on the central axis. Besides, the energy distribution of the coupled arc was more concentrated along *x*-axis, due to the compression of

arc shape, which was beneficial for the electrons to obtain more arc energy and caused an increase in the electron temperature on the central axis.

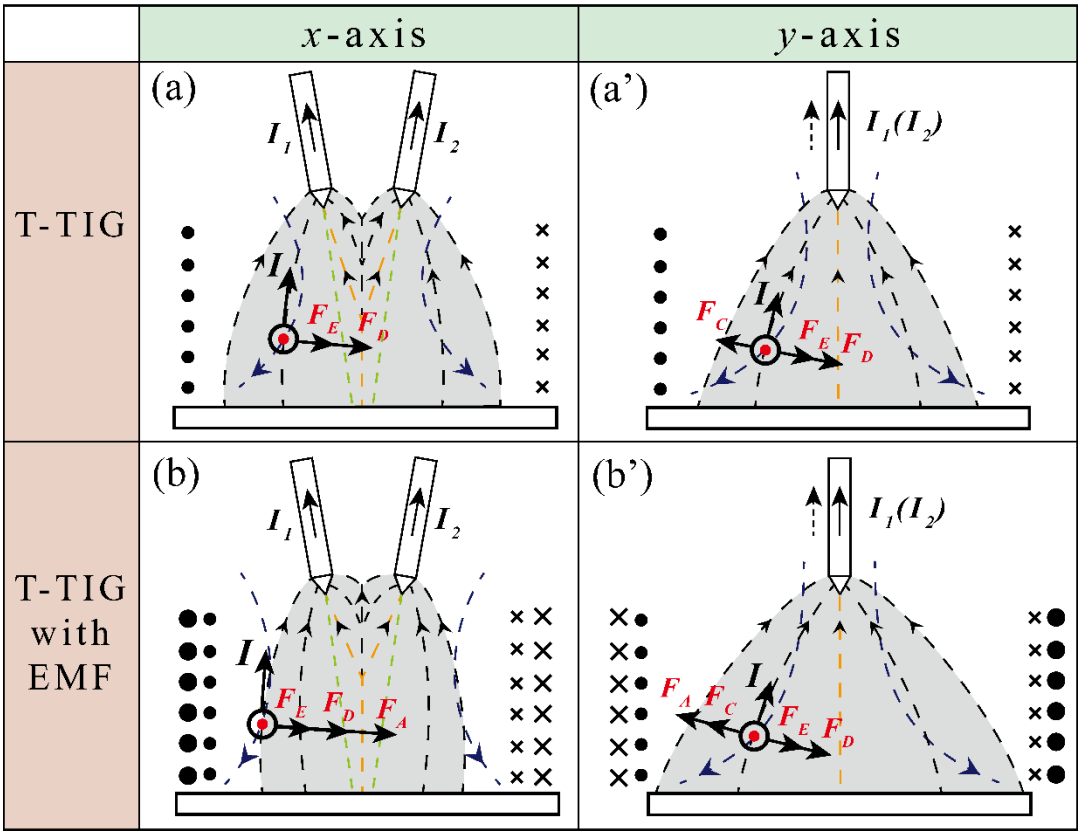

Fig. 15 Schematic of force analysis on *xOz* and *yOz* cross sections: **a,a'** T-TIG; **b,b'** T-TIG with EMF

However, along *y*-axis, the charged particles of T-TIG accelerated toward the periphery of the coupled arc under the effect of F_A, and then the coupled arc was elongated. Simultaneously, the strengthened collision on the central axis caused by the movement of the charged particles along *x*-axis led to an increase of the collision force F_C, which further accelerated the movements of the charged particles outward along *y*-axis. Therefore, the electron density on the central axis was decreased, while the electron density along *y*-axis was relatively increased and the movement velocities of the charged particles outward along *y*-axis were also increased, which also improved thermal movement of the electrons and caused the electron temperature along *y*-axis was increased. Additionally, the arc energy was dispersed

along *y*-axis due to the elongated arc shape, which reduced the electron temperature on the central axis.

Therefore, under the effect of the cusp EMF, considering the combining effect of the movement characteristics of the charged particles and the arc shape behaviour of T-TIG along *x*-axis and *y*-axis, electron temperature and electron density on the central axis were not increased significantly. However, along *y*-axis, the two parameters at each position of T-TIG were increased and the distribution range of the both were also increased obviously, which was beneficial to increase the melting efficiency of the filler wire fed along *y*-axis and thus further increased the deposition rate.

Conclusions

T-TIG assisted by a cusp EMF welding process was developed, and the influence of the cusp EMF on the deposition rate of T-TIG was studied. The specific conclusions were as follows:

1. Compared to TIG, T-TIG had low arc pressure characteristic, and thus a higher welding current could be allowed, which caused T-TIG had the potential to obtain higher deposition rate. Under the effect of the cusp EMF, the arc shapes of TIG and T-TIG were compressed along x-axis, while elongated along y-axis. Besides, the peak arc pressures of TIG and T-TIG were not significantly increased.

2. Under the effect of the cusp EMF, considering the combining effects of the movement characteristics of the charged particles and the arc shape behaviour along *x*-axis and *y*-axis of T-TIG, the increments of the T_e and N_e were gradually increased and the distributions of the two parameters were widened along *y*-axis of T-TIG, even though the T_e and N_e were not significantly increased on the central axis of T-TIG.

3. More arc energy was allocated on *y*-axis of T-TIG by the cusp EMF, which was beneficial to the melting efficiency of the filler wire fed along *y*-axis. Therefore, the deposition rate of T-TIG could be increased by 17.6% as the cusp EMF was applied.

Funding This work was supported by the National Key Research and Development Program of China(2018YFB1107900), and the National Natural Science Foundation of China (No. U1960111).

Author contribution Liming Liu: conceptualization, writing-review and editing.

Yanli Zhu: writing-original draft, methodology, formal analysis.

Runtao Liu: supervision, validation.

Data availability All the data have been presented in the manuscript.

Declarations

Ethics approval The paper follows the guidelines of the Committee on Publication Ethics (COPE).

Consent to participate The authors declare that they all consent to participate this research.

Consent for publication The authors declare that they all consent to publish the manuscript.

Competing interests The authors declare no competing interests.

References

1. Chen C, Xiao R, Chen H, Lv N, Chen S (2020) Arc sound model for pulsed GTAW and recognition of different penetration states. Int J Adv Manuf Technol 108: 3175-3191

2. Sarmast A, Serajzadeh S (2019) The influence of welding polarity on mechanical properties, microstructure and residual stresses of gas tungsten arc welded AA5052. Int J Adv Manuf Technol 105: 3397-3409

3. Kobayashi K, Yamada M, Fujishima K, Iijima T, Ushio M (2004) Development of high efficiency twin-arc TIG welding method. IIW Doc XII: 1669-1701

4. Kobayashi K, Nishimura Y, Iijima T, Ushio M, Tanaka M, Shimamura J, Ueno Y, Yamashita M (2004) Practical application of high efficiency twin-arc TIG welding method (SEDAR-TIG) for PCLNG storage tank. Weld World 48: 35-39

5. Leng X, Zhang G, Wu L (2006) The characteristic of twin-electrode TIG coupling arc pressure. J Phys D Appl Phys 39: 1120-1126
6. Leng X, Zhang G, Wu L (2006) Experimental study on improving welding efficiency of twin electrode TIG welding method. Sci Technol Weld Join 11: 550-554
7. Qin G, Meng X, Fu B (2015) High speed tandem gas tungsten arc welding process of thin stainless steel plate. J Mater Process Technol 220: 58-64
8. Jiang H, Qin G, Feng C, Meng X (2019) High-speed tandem pulsed GTAW of thin stainless steel plate. Weld J 98: 215-226
9. Wu D, Huang J, Kong L, Hua X, Wang M (2020) Coupled mechanisms of arc, weld pool and weld microstructures in high speed tandem TIG welding. Int J Heat Mass Transf 154: 119641
10. Nomura K, Morisaki K, Hirata Y (2009) Magnetic control of arc plasma and its modelling. Weld World 53: R181-R187
11. Liu Z, Chen S, Yuan X, Zuo A, Zhang T, Luo Z (2018) Magnetic-enhanced keyhole TIG welding process. Int J Adv Manuf Technol 99: 275-285
12. Liu S, Liu Z, Zhao X, Fan X (2020) Influence of cusp magnetic field configuration on K-TIG welding arc penetration behavior. J Manuf Process 53: 229-237
13. Zhu Y, Xu X, Liu R, Liu L (2021) Magnetic-enhanced common conductive channel characteristics of two-electrode TIG. Int J Adv Manuf Technol 116: 3217-3229
14. Lin ML, Eager TW (1985) Influence of arc pressure on weld pool geometry. Weld J 6: 163-169
15. Ogino Y, Hirata Y, Nomura K (2011) Numerical analysis of the heat source characteristics of a two-electrode TIG arc. J Phys D Appl Phys 44: 215-202
16. Mendez PF, Eagar TW (2003) Penetration and defect formation in high-current arc welding. Weld J 10: 296-306
17. Griem HR (1974) Spectral line broadening by plasmas. Academic Press, New York
18. Liu L, Hao X (2008) Study of the effect of low-power pulse laser on arc plasma and magnesium alloy target in hybrid welding by spectral diagnosis technique. J Phys D Appl Phys 41: 205202
19. Hao X, Song G (2009) Spectral analysis of the plasma in low-power laser/arc hybrid welding of magnesium alloy. IEEE Trans Plasma Sci 37: 76-82
20. Griem HR (1964) Plasma spectroscopy. McGraw-Hill, New York
21. Colón C, Alonso-Medina A (2006) Application of a laser produced plasma: experimental Stark widths of single ionized lead lines. Spectroc Acta Pt B-Atom Spectr 61: 856-863

22. Shea JE, Gardner CS (1983) Spectroscopic measurement of hydrogen contamination in weld arc plasmas. J Appl Phys 54: 4928-4938
23. Sabbaghzadeh J, Dadras S, Torkamany MJ (2007) Comparison of pulsed Nd: YAG laser welding qualitative features with plasma plume thermal characteristics. J Phys D Appl Phys 40: 1047-1051
24. National Institute of Standards and Technology Database. https://physics.nist.gov/PhysRefData/ASD/lines_form.html (accessed October 4, 2021)
25. Lin ML, Eagar TW (1986) Pressures produced by gas tungsten arcs. Metallurgical Transactions B 17: 601-607
26. Ueyama T, Ohnawa T, Tanaka M, Nakata K (2007) Occurrence of arc interaction in tandem pulsed gas metal arc welding. Sci Technol Weld Join 12: 523-529